



Itinerant antiferromagnetism in $\text{Co}_3\text{S}_{4-\delta}$ Liang-Wen Ji ¹, Yi Liu,^{1,2} Si-Qi Wu,¹ Bai-Zhuo Li,¹ Shi-Jie Song,¹ Yan-Wei Cui ^{1,3},
Zhi Ren,³ and Guang-Han Cao ^{1,4,5,*}¹*School of Physics, Zhejiang University, Hangzhou 310058, China*²*Department of Applied Physics, Zhejiang University of Technology, Hangzhou 310023, China*³*School of Sciences, Westlake Institute for Advanced Study, Westlake University, Hangzhou 310064, China*⁴*Collaborative Innovation Centre of Advanced Microstructures, Nanjing University, Nanjing 210093, China*⁵*Zhejiang Province Key Laboratory of Quantum Technology and Devices, Interdisciplinary Center for Quantum Information, and State Key Lab of Silicon Materials, Zhejiang University, Hangzhou 310058, China*

(Received 29 July 2022; revised 1 October 2022; accepted 6 October 2022; published 20 October 2022)

We present experimental and theoretical investigations for the cobalt thiospinel $\text{Co}_3\text{S}_{4-\delta}$. High-quality samples of $\text{Co}_3\text{S}_{4-\delta}$ ($\delta \sim 0.1$) were prepared so as to measure their intrinsic properties. The measurements of magnetic susceptibility, specific heat, and electrical transport consistently indicate an antiferromagnetic transition at ~ 60 K, which is attributed to long-range magnetic ordering in the Co(A) (A-site Co ions) diamond sublattice. In addition, there exists a short-range magnetic ordering at around 120 K associated with the magnetic frustrations. The high-temperature magnetic susceptibility obeys Curie-Weiss law, from which a small effective magnetic moment of $1.0 \mu_B$ per formula unit is yielded. The main experimental results can be interpreted by the density-functional-theory calculations with a Hubbard U correction of ~ 0.5 eV. Combining the experimental measurements with the theoretical calculations, we conclude that Co_3S_4 represents a rare example of itinerant-electron diamond-lattice antiferromagnet with moderate electron correlations.

DOI: [10.1103/PhysRevB.106.155138](https://doi.org/10.1103/PhysRevB.106.155138)**I. INTRODUCTION**

Transition-metal spinels exhibit diverse physical and chemical properties that are of both fundamental interest and technological applications [1–3]. Of particular interest are those thiospinels with partially filled d -shell cations, which can be either localized or delocalized with variable valence, depending on the specific system and external conditions. In a normal thiospinel with the chemical formula of AB_2S_4 , A and B cations occupy the tetrahedral and octahedral sites, respectively, forming diamond and pyrochlore lattices prone to strong frustration effects [3]. Co_3S_4 , which occurs in nature as the mineral linneite, crystallizes in the normal spinel structure, in which Co ions occupy both A and B sites [4]. The Co ions on the B site, denoted as Co(B), are nonmagnetic (NM) because of the low-spin state similar to the case in Co_3O_4 [5,6]. However, the magnetic state of Co(A) ions in Co_3S_4 is very different from that of Co_3O_4 , the former of which still remains elusive at present. Note that the A -site ions form a diamond lattice, which could exhibit a novel spin-liquid state [3,7–9]. Thus the magnetism of Co_3S_4 are of particular interest for exploring exotic states of matter.

Although there have been lots of studies focusing on the application aspects [10–13], surprisingly few studies were carried out on the bulk properties of Co_3S_4 , and the fundamental properties have remained unclear for decades. In the 1960s, Heidelberg *et al.* [14] showed that the magnetic susceptibility

of $\text{Co}_3\text{S}_{4-\delta}$ was temperature independent above 400 K. Such a temperature-independent susceptibility of $\sim 10^{-3}$ emu/mol, which was very sensitive to the purity of the sample, was extended down to 100 K [15] or 20 K [1]. Meanwhile, metallic conductivity above 90 K was reported for Co_3S_4 [16]. The small value of magnetic susceptibility together with the metallic conduction suggests a simple Pauli paramagnetic state, in which the $3d$ electrons of Co(A) atoms are totally delocalized.

In 1991, however, Nishihara *et al.* [17] suggested that the Co(A) ions undergo a magnetic ordering at 58 K from the ^{59}Co NMR measurement. At the same period, an unpublished neutron scattering study, quoted in Ref. [18], showed a weak antiferromagnetism below 55 K for Co(A) ions with a very small magnetic moment of $\mu_{\text{Co}(A)} = 0.3 \mu_B$. Nevertheless, no direct evidence of the AFM transition could be observed in the magnetic susceptibility [17]. From our recent study on the related cobalt thiospinel of CuCo_2S_4 [19], we judged that the situation is likely to be owing to the existence of small amount of the ferromagnetic impurity of CoS_2 in the Co_3S_4 sample studied.

Motivated by exploration of unconventional superconductivity in cobalt-based systems, we recently demonstrated that CuCo_2S_4 exhibits bulk superconductivity [19]. This work inspires us to study its sibling material Co_3S_4 , for resolving the issue of magnetism above and, for exploring the possible unconventional superconductivity as well. By employing the synthesis strategy developed earlier [19], in the present work, we succeeded in preparing sulfur-deficient $\text{Co}_3\text{S}_{4-\delta}$ ($\delta \sim 0.1$) samples that are free of CoS_2 impurity. The intrinsic physical properties of $\text{Co}_3\text{S}_{4-\delta}$ were thus measured, from which an

*ghcao@zju.edu.cn

AFM transition at ~ 60 K, short-range magnetic ordering at around 120 K, and Curie-Weiss paramagnetic behavior at high temperatures are revealed. The results are in sharp contrast with the NM analog $\text{NiCo}_2\text{S}_{4-\delta}$ [1,20]. We also performed the density-functional-theory (DFT) calculations. The effect of Hubbard U parameter on the ground state was systematically investigated, which suggests a realistic $U \sim 0.5$ eV for Co_3S_4 . The magnetic and electronic properties were calculated with inclusion of this Hubbard U correction. Our results indicate that Co_3S_4 is an itinerant-electron diamond-lattice antiferromagnet with moderate electron correlations, which is close to a quantum critical point (QCP).

II. EXPERIMENTAL METHODS AND DFT CALCULATIONS

Polycrystalline samples of $\text{Co}_3\text{S}_{4-\delta}$ were synthesized by high-temperature solid-state reactions in sealed silica ampoule [16,19]. The source materials were powders of Co (99.9%) and S (99.999%), which were mixed with the composition of $\text{Co}_3\text{S}_{4-\delta}$ ($\delta = 0-0.2$) and heated at 530–540 °C for 48 h. The solid-state reactions were repeated several times with intermediate grindings, which improved the sample quality. We also prepared single-phase samples of $\text{NiCo}_2\text{S}_{4-\delta}$ as the NM analog of $\text{Co}_3\text{S}_{4-\delta}$ for comparison. The solid-state reaction temperature was 600 °C, and the best sample was obtained with the nominal composition of $\text{NiCo}_2\text{S}_{3.9}$. Note that operations of weighing, grinding, pressing, and loading of samples were all carried out in a glove box filled with high-purity argon.

The polycrystalline sample was examined by powder x-ray diffractions (XRD) using a PANalytical diffractometer with a monochromatic $\text{Cu-K}\alpha_1$ radiation. The crystal structures were refined by a Rietveld analysis using the RIETAN-FP package [21]. The dc magnetization was measured on a Quantum Design Magnetic Property Measurement System (MPMS3). The magnetic susceptibility was measured up to 600 K using the high-temperature option. The transport properties and heat capacity were measured on a Quantum Design Physical Properties Measurement System (PPMS-9). The resistivity and Hall measurement employed standard four-terminal methods, and the heat-capacity measurement utilized a thermal relaxation technique.

Our DFT calculations were performed using the projector augmented wave (PAW) method [22], implemented in the VASP package [23]. We adopted the generalized gradient approximation (GGA) in the Perdew, Burke, and Enzerhoff scheme to treat with the exchange-correlation energy [24]. An energy cutoff of 450 eV for the basis expansion and the Hubbard U correction (GGA + U) [25] for the Co-3d orbitals was employed. The calculations were conducted on the 14-atoms primitive cell for Co_3S_4 thiospinel, and a $8 \times 8 \times 8$ Γ -centered k mesh was adopted for the self-consistent calculations. The atomic positions and lattice parameters were relaxed until the atomic forces are less than 0.003 eV/Å. The calculated lattice parameter is $a_0 = 6.5642$ Å, corresponding to the conventional unit cell with $a = \sqrt{2}a_0 = 9.2832$ Å. This relaxed lattice parameter is 1.3% smaller than the experimental value for $\text{Co}_3\text{S}_{3.88}$ measured at room temperature (see below). The u parameter, which determines the coordinates of

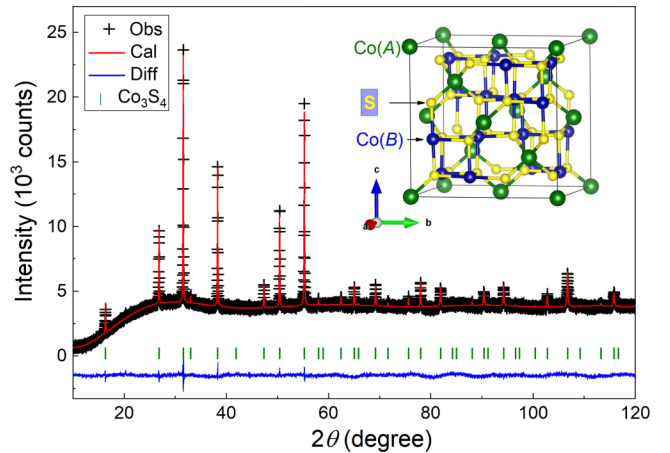


FIG. 1. Powder x-ray diffraction and its Rietveld refinement profile for the sample with nominal composition of $\text{Co}_3\text{S}_{3.91}$. The inset shows the crystal structure.

sulfur atoms at (u, u, u) , is calculated to be 0.3821, exactly coincident with the experimental result. To precisely calculate the contributions from different atomic orbitals in Co_3S_4 , we constructed a tight-binding Hamiltonian with 108 atom-centered Wannier orbitals (60 Co-3d and 48 S-3p orbitals) [26].

III. RESULTS AND DISCUSSION

A. Structure characterization

We prepared a series of $\text{Co}_3\text{S}_{4-\delta}$ samples with $\delta = 0-0.2$. For $\delta \leq 0.06$, the samples always contain significant amount of CoS_2 ferromagnetic impurity, which severely interferes with the magnetic property measurement. In the case of $\delta \geq 0.15$, the secondary phase of Co_{1-x}S appears, as detected by the XRD (not shown here). Single-phase samples of $\text{Co}_3\text{S}_{4-\delta}$ can be obtained with $\delta \approx 0.1$ (postsulfurization always yields the undesired secondary phase of CoS_2). Figure 1 shows the XRD data of the sample with the nominal composition of $\text{Co}_3\text{S}_{3.91}$. While there is large background noise due to the existence of cobalt element in the sample, the diffraction intensities are remarkable, indicating good crystallinity. In particular, no secondary phases of CoS_2 and Co_{1-x}S are detectable within the limit of the XRD measurement. The Rietveld refinement was very successful with pretty small R factors and acceptable goodness-of-fit parameter S (see Table I).

TABLE I. Crystal structure of $\text{Co}_3\text{S}_{4-\delta}$ at room temperature from the Rietveld refinement of powder x-ray diffraction.

S.G.	a (Å)	V (Å ³)	R_{wp} (%)	R_{p} (%)	S
$Fd\bar{3}m$	9.4063(3)	832.25(4)	2.87	2.16	1.74
Atoms	x	y	z	Occ.	B (Å ²)
Co(A)	1/4	1/4	1/4	1.00	0.60(9)
Co(B)	5/8	5/8	5/8	1.00	0.59(10)
S	0.3820(2)	0.3820(2)	0.3820(2)	0.971(9)	0.39(10)

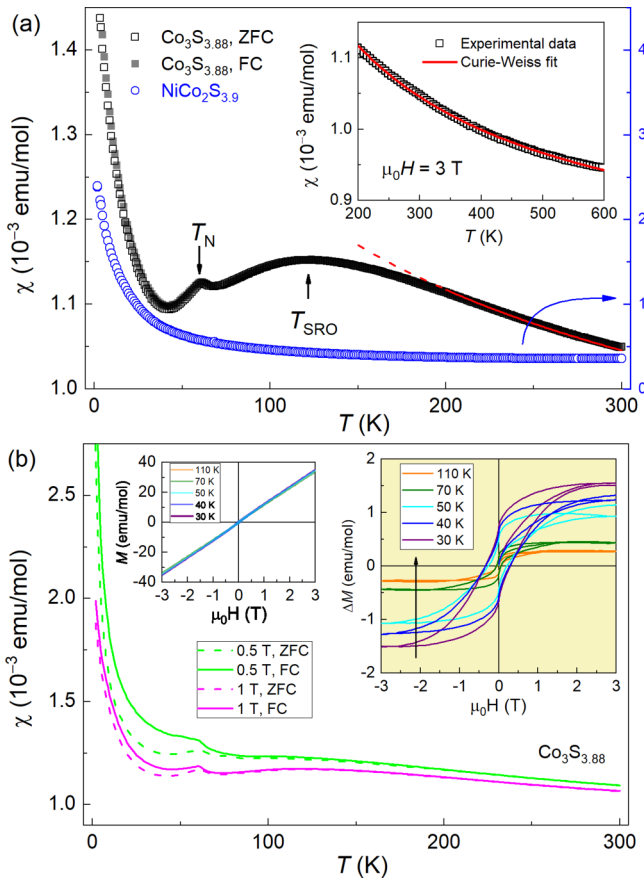


FIG. 2. (a) Temperature dependence of magnetic susceptibility for $\text{Co}_3\text{S}_{3.88}$ (left axis) and $\text{NiCo}_2\text{S}_{3.9}$ (right axis) with an applied field of $\mu_0 H = 3$ T. The inset shows the high-temperature susceptibility data together with the Curie-Weiss fitting for $\text{Co}_3\text{S}_{3.88}$. (b) Temperature dependence of magnetic susceptibility for $\text{Co}_3\text{S}_{3.88}$ at lower fields of $\mu_0 H = 0.5$ and 1 T in the zero-field-cooling (ZFC) and field-cooling (FC) processes. The left inset shows the isothermal magnetization at fixed temperatures. The right inset plots the non-linear portion of the magnetization, $\Delta M = M - \chi H$.

The lattice parameter refined is $a = 9.4063(3)$ Å, which is closely consistent with that [$9.4055(12)$ Å] of the previous report for Co_3S_4 [4]. We note that our samples of $\text{Co}_3\text{S}_{4-\delta}$ with $\delta = 0-0.06$ have essentially the same lattice constant, containing small amount of CoS_2 impurity as stated above. The result suggests that any nominal Co_3S_4 sample prepared by solid-state reactions has a certain sulfur deficiency. According to our Rietveld analysis, indeed, the sulfur occupation fraction in the sample $\text{Co}_3\text{S}_{3.91}$ is $0.971(9)$, which means that the actual composition is $\text{Co}_3\text{S}_{3.88}$ (there was reasonably loss of sulfur during the preparation of samples). Besides, the structural parameter $u = 0.3820(2)$ is not far from the ideal value of 0.375 , indicating only slight distortion of the CoS_6 octahedra along the $\langle 111 \rangle$ direction.

B. Magnetism

Figure 2(a) shows the temperature dependence of magnetic susceptibility for $\text{Co}_3\text{S}_{3.88}$ and, for the reference sample $\text{NiCo}_2\text{S}_{3.9}$ as well for comparison. The possible ferromagnetic

signal at ~ 120 K from the CoS_2 impurity [27] cannot be directly seen (the upper limit of the fraction of CoS_2 is estimated to be $\sim 1/10000$, according to the method in our previous work [19]). Hence the susceptibility measured reflects the intrinsic properties [28]. One clearly sees that the magnetic behaviors of $\text{Co}_3\text{S}_{3.88}$ and $\text{NiCo}_2\text{S}_{3.9}$ are contrastingly different. While the $\chi(T)$ data of $\text{NiCo}_2\text{S}_{3.9}$ are basically temperature independent, the $\chi(T)$ curve of $\text{Co}_3\text{S}_{3.88}$ shows a cusp at $T_N = 62$ K, a hump centered at ~ 120 K, and a Curie-Weiss paramagnetic behavior at high temperatures.

The susceptibility cusp in $\text{Co}_3\text{S}_{3.88}$ is likely to be due to an AFM ordering, coincident with the 58-K anomaly in the NMR experiment [17]. The broad hump is probably associated with short-range ordering (SRO) of magnetic moments, thus we define the susceptibility-maximum temperature as T_{SRO} . Such an SRO commonly appears in low-dimensional and/or magnetically frustrated systems. Here, the Co(A) ions in Co_3S_4 form a diamond lattice, which renders magnetic frustrations in relation with bond order [3,7,8].

The Curie-Weiss behavior at high temperatures contrasts with the earlier reports [14,15] that showed temperature independence of the magnetic susceptibility. As is shown in the inset of Fig. 2(a), the high-temperature susceptibility obeys the Curie-Weiss law, $\chi = \chi_0 + C/(T - \theta_W)$. The Curie-Weiss fit yields a temperature-independent susceptibility of $\chi_0 = 7.81 \times 10^{-4}$ emu/mol, a Curie constant of $C = 0.124$ emu K/mol, and a Weiss temperature of $\theta_W = -170$ K. In general, χ_0 may be contributed from core-electron diamagnetism, Pauli paramagnetism, Landau diamagnetism (equal to $-1/3$ of Pauli paramagnetism), and Van Vleck paramagnetism. The core-electron susceptibility is estimated to be -1.48×10^{-4} emu/mol [29], which almost cancels out the Pauli paramagnetic contribution [$\chi_P = \mu_B^2 N(E_F) = 1.36 \times 10^{-4}$ emu/mol] derived from the first-principles calculations (see below). Thus the relatively large value of χ_0 should be dominantly contributed from the Van Vleck paramagnetism of the B-site Co ions, similar to the case in CuCo_2S_4 [30].

With the fitted Curie constant C , the effective magnetic moment is calculated to be $p_{\text{eff}} = 1.00 \mu_B/\text{f.u.}$ (f.u. denotes formula unit), using the formula $p_{\text{eff}} = \sqrt{\frac{3k_B C}{N_A \mu_B^2}} \approx \sqrt{8C}$ ($\mu_B/\text{f.u.}$), where k_B and N_A are Boltzmann constant and Avogadro constant, respectively. The effective magnetic moment only accounts for 58% of the effective localized moment of $2\sqrt{S(S+1)} = 1.73 \mu_B$ with the lowest quantum spin of $S = 1/2$. Note that the effective moment of Co_3O_4 is $4.80 \mu_B/\text{Co(A)}$, and the Co(A) ions are completely localized with a local spin of $S = 3/2$ [6]. The remarkably reduced p_{eff} in $\text{Co}_3\text{S}_{3.88}$ strongly suggests that the electrons on Co(A) atoms are itinerant. The negative θ_W value indicates dominant AFM correlations, consistent with the deviation from Curie-Weiss law as well as the susceptibility hump below 200 K. The frustration parameter $f = |\theta_W|/T_N = 2.74$ suggests a moderate frustration [3].

Here we note that the susceptibility hump as well as the AFM transition is accompanied with a tiny ferromagnetic (FM) polarization. Figure 2(b) shows the magnetic susceptibility of $\text{Co}_3\text{S}_{3.88}$ at lower fields of $\mu_0 H = 0.5$ and 1 T. Bifurcation of the zero-field-cooling (ZFC) and

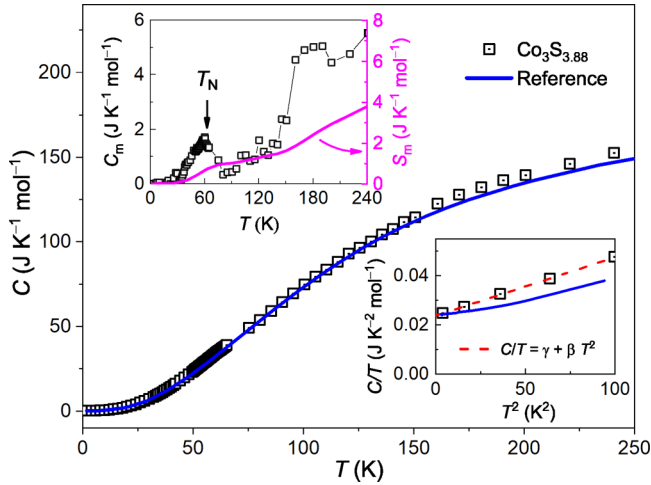


FIG. 3. Specific heat C as a function of temperature for $\text{Co}_3\text{S}_{3.88}$. The reference data (blue line), converted from those of $\text{NiCo}_2\text{S}_{3.9}$, represent the nonmagnetic contribution, C_{nm} . The magnetic contribution, $C_m = C - C_{\text{nm}}$, is shown in the upper inset, and the magnetic entropy $S_m = \int_0^T \frac{C_m}{T} dT$ is plotted (in magenta color) using the right axis. The lower inset plots C/T versus T^2 in the low-temperature regime.

field-cooling (FC) curves can be seen below ~ 200 K, which is enhanced below T_N . Nevertheless, the FM signal is so small that the isothermal magnetization, $M(H)$, is basically linear even at $T < T_N$ [see the left inset of Fig. 2(b)]. With the deduction of the linear magnetization, χH , the remaining non-linear portion displays an FM-like hysteresis [the right inset of Fig. 2(b)]. The ordered moment is only ~ 1 emu/mol, equivalent to $\sim 2 \times 10^{-4} \mu_B/\text{f.u.}$ The result indicates that the magnetic ground state is virtually AFM in nature. The magnetic hysteresis that appears at $T > T_N$ suggests that the SRO state is something like cluster-spin glass. Remember that the frustration parameter in the present system is not so large, hence the susceptibility hump is not only due to the bond-order frustration, but also probably due to long-range Ruderman-Kittel-Kasuya-Yosida (RKKY) exchange interactions that appear exclusively in a metallic system.

C. Specific heat

To get more information about the magnetic and electronic properties, we measured the specific heat of the identical $\text{Co}_3\text{S}_{3.88}$ sample. Let us first analyze the low-temperature data. According to Debye law, the low-temperature specific heat can be expressed by $C/T = \gamma + \beta T^2$, from which the electronic specific heat can be separated out. As shown in the lower inset of Fig. 3, C/T is essentially linear with T^2 , and the linear fit gives an intercept of $\gamma = 23.8 \text{ mJ K}^{-2} \text{ mol}^{-1}$ and a slope of $\beta = 0.238 \text{ mJ K}^{-4} \text{ mol}^{-1}$ for $\text{Co}_3\text{S}_{3.88}$. The reference data derived from the NM $\text{NiCo}_2\text{S}_{3.9}$ (the blue line, see below) show a similar γ value, but a reduced β value. The enhanced β value for $\text{Co}_3\text{S}_{3.88}$ suggest significant contributions from the AFM magnons.

Second, one notes that there is no obvious anomaly at T_N or T_{SRO} in the raw data of $\text{Co}_3\text{S}_{3.88}$. In order to extract the magnetic contributions, we employed the specific-heat

data of the NM analog $\text{NiCo}_2\text{S}_{3.9}$, which appear to be systematically lower than those of $\text{Co}_3\text{S}_{3.88}$. Thus we made a correction according to the literature [31], simply by rescaling the temperature with $T^* = \frac{T}{(M_{\text{Co}_3\text{S}_{3.88}}/M_{\text{NiCo}_2\text{S}_{3.9}})^{1/2}}$, where M is their individual molecular weight. The corrected $C(T)$ data are shown in Fig. 3 (the blue line), which approximately represents the NM contribution in $\text{Co}_3\text{S}_{3.88}$, C_{nm} . Then, the magnetic contribution of $\text{Co}_3\text{S}_{3.88}$ was obtained by the subtraction, $C_m = C - C_{\text{nm}}$. As shown in the top inset of Fig. 3, there are two peaks at ~ 60 K and ~ 180 K in the $C_m(T)$ data extracted. The first one coincides with the cusp in magnetic susceptibility at T_N , verifying the long-range magnetic ordering. The magnetic entropy released at the magnetic transition is about $0.8 \text{ J K}^{-1} \text{ mol}^{-1}$, which is only 1/10 of the value of $R \ln 2$ ($S = 1/2$), suggesting significant residual magnetic entropy above T_N due to the SRO. Indeed, the magnetic entropy released at 240 K achieves $3.8 \text{ J K}^{-1} \text{ mol}^{-1}$, which accounts for half of $R \ln 2$. This result is consistent with the small effective moment of $p_{\text{eff}} = 1.00 \mu_B/\text{f.u.}$, further confirming the itinerant nature for the Co(A) electrons.

D. Transport properties

Figure 4(a) shows the temperature dependence of electrical resistivity for the $\text{Co}_3\text{S}_{3.88}$ and $\text{NiCo}_2\text{S}_{3.9}$ polycrystalline samples. As the NM analog, $\text{NiCo}_2\text{S}_{3.9}$ shows a normal metallic behavior with linear temperature dependence of resistivity in the high-temperature regime, basically consistent with the previous report [20]. For $\text{Co}_3\text{S}_{3.88}$, while it is also metallic with similar resistivity values in the whole temperature range, details of the $\rho(T)$ curve differ. First, the $\rho(T)$ curve exhibits a convex behavior above ~ 100 K. Second, there is an anomaly at ~ 60 K. Obviously, these extra features dictate the magnetic scattering effect. Thus we plotted the $\rho(T)$ difference between the two samples in the inset of Fig. 4(a), which clearly shows a jump at ~ 60 K and a hump at around ~ 120 K. The resistivity jump at T_N should be attributed to the AFM ordering, while the resistivity hump at T_{SRO} arises from the SRO of Co(A) spins mentioned above. Additional evidence of the AFM transition at T_N is given by the temperature dependence of magnetoresistance, $\text{MR} = (\rho_{3T} - \rho_{0T})/\rho_{0T}$, shown in the right inset of Fig. 4(a). Although there is nearly zero MR above T_N , significantly large MR develops below T_N . The positive MR effect further supports the AFM (rather than FM) ordering.

Figure 4(b) shows the temperature dependence of Hall coefficient (R_H), extracted from the raw data shown in the inset, for the $\text{Co}_3\text{S}_{3.88}$ sample. As we know, R_H is normally temperature independent for a single-band NM metal. Here we see that R_H is strongly temperature dependent and, it even changes the sign, both of which indicate a multiband character in which hole-type carriers dominate the electrical transport at low temperatures. One notes that the sign change coincides with the SRO of Co(A) spins, implying the relevance of magnetic ordering to the electronic structure. With decreasing temperature to T_N , R_H increases steeply, which means a decrease in carrier density, corresponding to the resistivity jump above. The fact that the transport properties intimately couple with the magnetism further corroborates the itinerant-electron scenario.

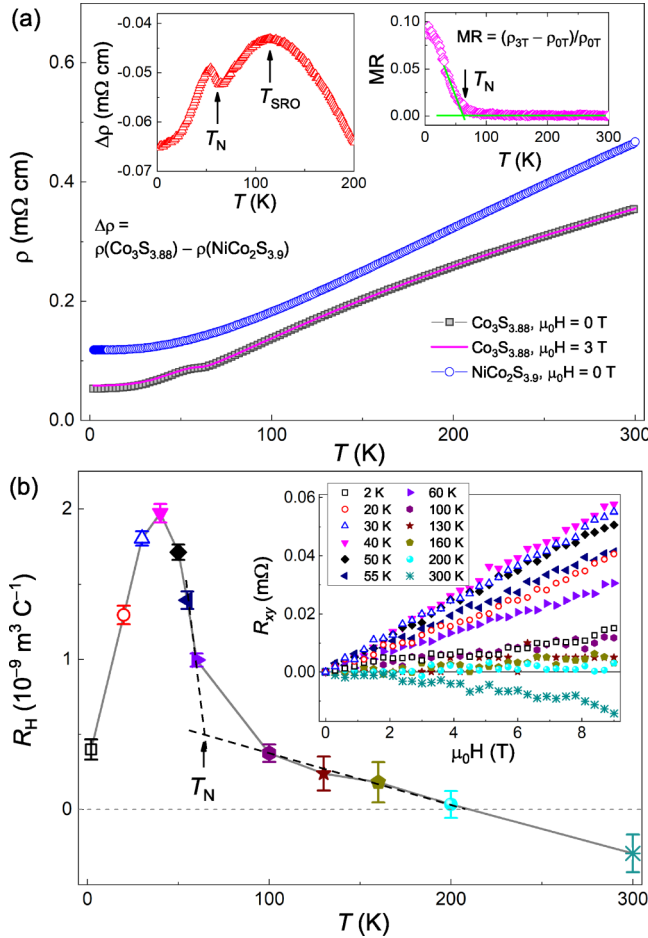


FIG. 4. (a) Temperature dependence of electrical resistivity for the $\text{Co}_3\text{S}_{3.88}$ and $\text{NiCo}_2\text{S}_{3.9}$ polycrystalline samples. The left inset plots the resistivity difference between two samples, and the right inset shows the magnetoresistance (MR) of $\text{Co}_3\text{S}_{3.88}$. (b) Temperature dependence of Hall coefficient for $\text{Co}_3\text{S}_{3.88}$. The inset shows the field dependence of Hall resistance at fixed temperatures labeled.

E. Magnetic and electronic structures

There have been a few first-principles calculations on the cobalt thiospinel Co_3S_4 [11–13,18,32]. Miyazaki *et al.* [18] reported the first electronic band structure calculations for Co_3S_4 , which gives a metallic AFM state with $\mu_{\text{Co}(A)} = 0.3 \mu_B$ and the AFM propagation wave vector of $\mathbf{q} = 0$. Namely, the Co(A) spins order antiferromagnetically between the two interpenetrating face-centered cubic lattices, which is commonly seen for a diamond spin lattice [3]. In recent years, the DFT calculations were conducted by taking the Hubbard U correction into account, which yield distinct results [11–13,32]. Wang *et al.* [12] concluded zero band gap with $\mu_{\text{Co}(A)} = 2.04 \mu_B$ under $U = 2$ eV. Ge *et al.* [11] obtained a small bandgap of $E_g = 0.1$ eV at $U = 4.4$ eV. Samal *et al.* [13] concluded $\mu_{\text{Co}(A)} = 2.55 \mu_B$ and $E_g \approx 0.7$ eV for $U_{\text{eff}} = 6.5$ eV. And finally, Kim *et al.* [32] obtained a larger indirect band gap of $E_g = 1.02$ eV with $\mu_{\text{Co}(A)} = 2.71 \mu_B$ under $U_{\text{eff}} = 6.7$ eV. In a word, the calculation results strongly depend on the U values adopted. Therefore, it is critical to find a realistic U for the understanding of the magnetic and electronic structures of Co_3S_4 .

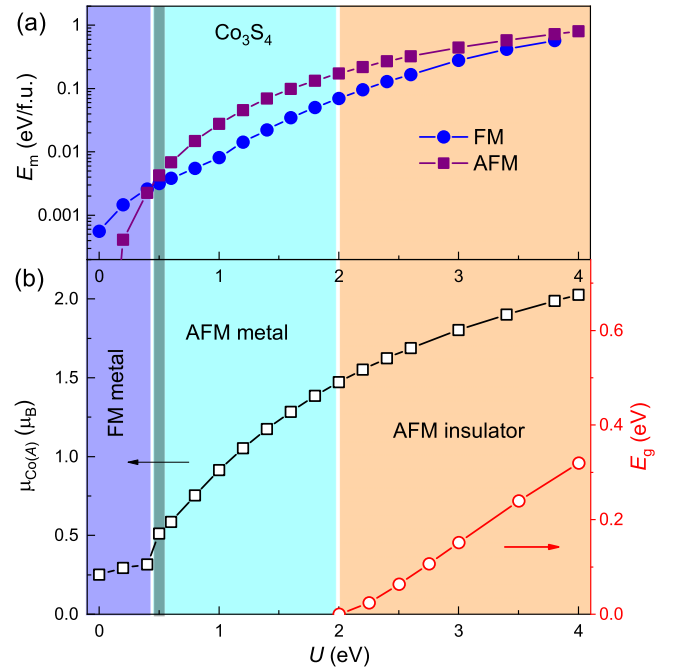


FIG. 5. (a) Magnetic energy, $E_m = E_{\text{NM}} - E_{\text{M}}$, of the ferromagnetic (FM) and antiferromagnetic (AFM) states of Co_3S_4 as functions of U in the GGA + U calculations. (b) Magnetic moment at the Co(A) site, $\mu_{\text{Co}(A)}$ (left axis), and band gap E_g (right axis) of the three ground states, FM metal, AFM metal, and AFM insulator. The gray dark stripe marks the realistic state for Co_3S_4 .

Effect of parameter U . We first calculated the total energies of NM, FM, and AFM states with varied U . We found that the energies of FM and AFM phases are always lower than that of the NM state for $U < 4.0$ eV. Figure 5(a) shows the absolute values of energies of the magnetic phases relative to that of the NM state, $E_m = E_{\text{NM}} - E_{\text{M}}$. In the small U regime with $U \leq 0.4$ eV, the ground state appears to be FM, different from the earlier report [18]. For $U \geq 0.5$ eV, the AFM state is stabilized. It should be noted that, for $U \leq 0.5$ eV, there are no obvious differences (less than 5 meV/f.u.) in the total energy between FM, AFM, and NM states. This suggests a magnetic QCP connecting the AFM, FM, and NM phases.

Our calculations show that nonzero magnetic moments appear only at the Co(A) site. The magnetic moment of Co(A) ions, $\mu_{\text{Co}(A)}$ is found to increase monotonically with U , as shown in Fig. 5(b). In the FM region, $\mu_{\text{Co}(A)}$ increases slowly up to $0.32 \mu_B$ at $U = 0.4$ eV. Upon entering the AFM regime, $\mu_{\text{Co}(A)}$ jumps to $0.51 \mu_B$ at $U = 0.5$ eV, and then it increases steadily to $1.5 \mu_B$ at $U = 2.0$ eV where a metal-to-insulator transition occurs. No abrupt change in $\mu_{\text{Co}(A)}$ is seen at the phase boundary. The band gap of the AFM insulator increases almost linearly with U , basically consistent with the previous calculations [12,13,32]. The result suggests an important role of Mottness for the metal-to-insulator transition. Considering the AFM metallic ground state with an effective magnetic moment of $p_{\text{eff}} = 1.0 \mu_B/\text{Cr}(A)$, which corresponds to an ordered moment of $0.41 \mu_B$ (assuming a spin-only scenario), we suggest that the realistic U value is ~ 0.5 eV. Note that a similarly small value of $U \leq 1$ eV is concluded

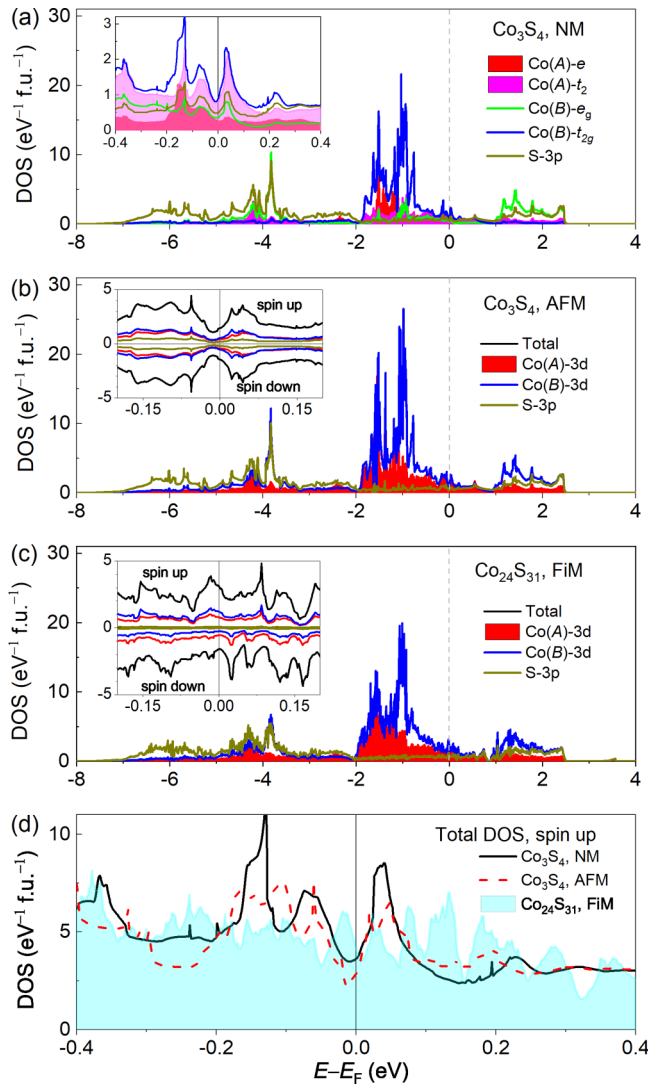


FIG. 6. Projected density of states (DOS) as a function of energy (relative to the Fermi energy E_F) for nonmagnetic (NM) Co_3S_4 (a), antiferromagnetic (AFM) Co_3S_4 (b), and ferrimagnetic (FiM) $\text{Co}_{24}\text{S}_{31}$ (c). The insets show the closeups at around E_F . The total DOS nearby E_F for the three cases are compared in (d). In the GGA + U calculations, the U value is set to be 0.5 eV.

for the itinerant ferromagnet CoS_2 [33], a closely relative compound of Co_3S_4 . In the following calculations, the U parameter is set to be 0.5 eV for interpreting the experimental results.

Electronic properties of the NM state. Figure 6(a) depicts the partial density of states (DOS) projected to each atomic orbital for NM Co_3S_4 . The electronic states are mainly contributed by Co-3d and S-3p orbitals. Among them, Co(B)- e_g orbitals strongly hybridize with the S-3p ones, while the hybridizations between Co(A)- t_2 and S-3p orbitals are moderate. Other Co-3d orbitals, Co(A)- e and Co(B)- t_{2g} , are basically in nonbonding states, which are almost filled. Thus Co(B) ions are in the low-spin state with zero magnetic moment. On the other hand, the Co(A)- t_2 orbitals are partially occupied, yet the occupation fraction is much higher than half (which is the case for Co_3O_4 [6]) because of the $t_2 - p$ hybridizations.

Note that the Fermi level lies in the dominantly nonbonding states mainly contributed from Co(A)- t_2 and Co(B)- t_{2g} orbitals [see the inset of Fig. 6(a)]. The total DOS for both spins at E_F is $N(E_F) = 3.62 \text{ eV}^{-1} \text{ f.u.}^{-1}$, corresponding to an electronic specific-heat coefficient of $\gamma_0 = \frac{1}{3}\pi^2 k_B^2 N(E_F) = 8.54 \text{ mJ K}^{-2} \text{ mol}^{-1}$. The γ_0 value derived from bare DOS is only about one-third of the experimental one ($\gamma = 23.8 \text{ mJ K}^{-2} \text{ mol}^{-1}$) from the specific-heat measurement, primarily because of the effective mass enhancements from electron-phonon coupling and electron-electron interactions. Since the electron-phonon coupling alone cannot account for the effective mass enhancement, one expects that electron correlation effect also plays a significant role for the mass renormalization of the itinerant electrons.

The band structures of the NM Co_3S_4 are shown in Figs. 7(a) and 7(d). There are three bands crossing the Fermi level, yielding three Fermi-surface sheets (FSSs) shown in Fig. 7(b). The FSS of the α band comprises small round-shape hole pockets centered around the L points. The FSS from the β band is also holelike with additional shadow pockets around X points. The third FSS is derived from the γ band, appearing around the edge centers (K/U points) of the Brillouin zone. Importantly, it is of electron type. In Fig. 7(d), one sees that the Co(B)- t_{2g} orbitals mainly contribute the X-point centered hole pockets, while the Co(A)- t_2 orbitals contribute both the hole-type and electron-type FSSs. The complex multiband feature seems to be responsible for the Hall measurement result with dominant hole-type conduction.

Effect of AFM ordering. The electronic DOS for the AFM Co_3S_4 is shown in Fig. 6(b). For simplicity, the contributions from $t_{2g}(t_2)$ and $e_g(e)$ are not separately displayed here. One sees that the DOS spectrum is basically the same as that of the NM state, primarily because of the small magnetic moment involved in the AFM order. E_F locates nearby a dip, similar to the NM case. The $N(E_F)$ value decreases significantly [$\sim 20\%$, see Fig. 6(d)], which accounts for the anomalies at T_N in the resistivity and Hall coefficient measurements.

As shown in Figs. 7(a) (dashed red lines) and 7(c), indeed, the band structures of the AFM Co_3S_4 are quite similar to the counterparts of the NM state. Nevertheless, the AFM state owns smaller FSSs [Fig. 7(c)], which also explains the anomalies in the resistivity and Hall coefficient measurements. In particular, the temperature-dependent Hall coefficient with sign change at $\sim 200 \text{ K}$ can be qualitatively explained by the larger FSSs for the NM state (i.e., in the high-temperature regime). It is also noted that, similar to the NM state, the Co(A)- t_2 orbitals contribute both the hole-type and electron-type FSSs in the AFM state. That is to say, the Co(A)- t_2 electrons are itinerant with nonzero magnetic moment.

Effect of sulfur deficiency. To match with the experimental result, we conducted additional calculations with sulfur deficiency using a supercell approximation. By assigning a sulfur vacancy at the (u, u, u) site of the conventional unit cell (note that the supercell has the same size with the conventional unit cell), one obtains a chemical formula of $\text{Co}_{24}\text{S}_{31}$, which is identical to $\text{Co}_3\text{S}_{3.875}$, very close to the experimental one. As shown in Fig. 6(c), while the basic features of the spectrum remain the same, the DOS for up and down spins are not

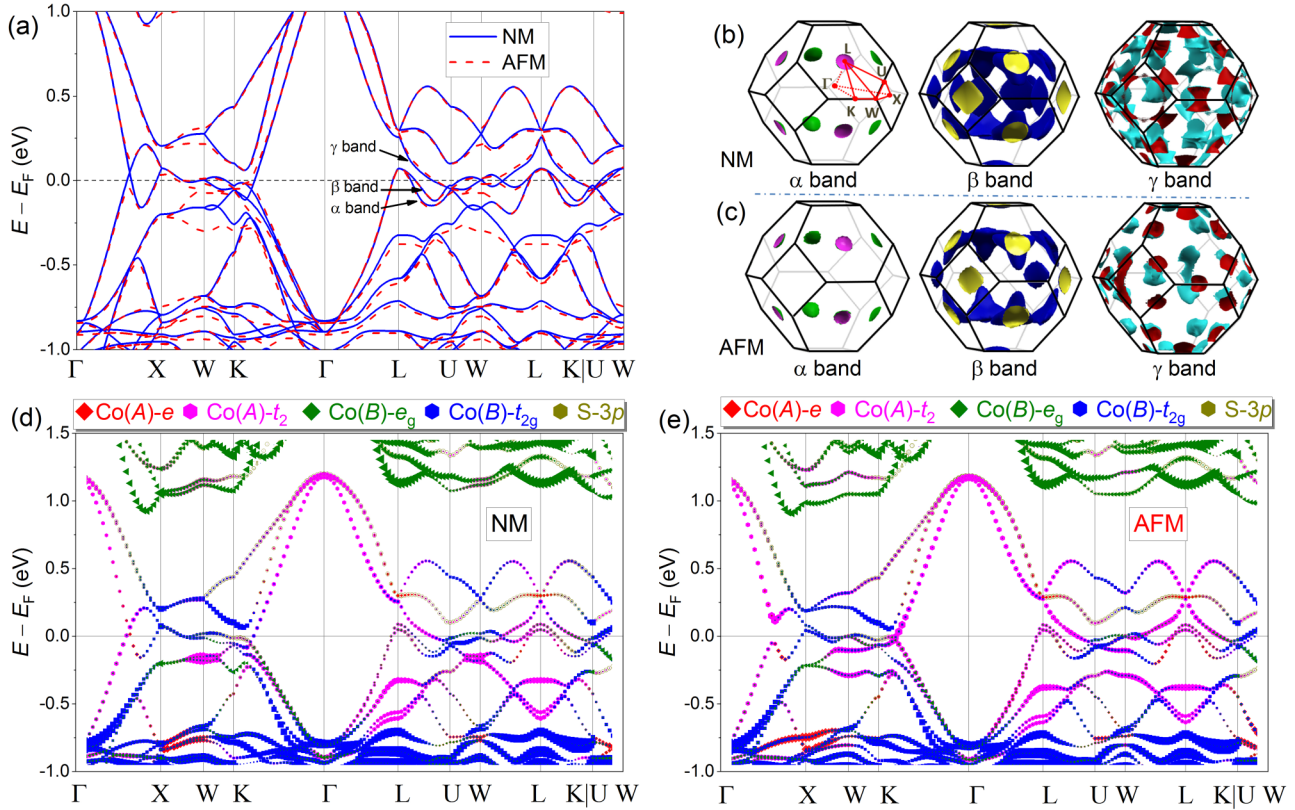


FIG. 7. (a) Electronic band structures for nonmagnetic (NM) and antiferromagnetic (AFM) Co_3S_4 . The Fermi surface sheets of the NM and AFM states are displayed in (b) and (c), with the high-symmetry points indicated in the upper-left Brillouin zone. The band structure contributions from different valence orbitals for the NM and AFM states are shown in (d) and (e), respectively.

symmetric any longer [see the inset of Fig. 6(c)], and an FM polarization of $\sim 0.2 \mu_B/\text{f.u.}$ is generated. The FM component mainly comes from the uncompensated magnetic moment at Co(A). Thus the calculated ground state of $\text{Co}_3\text{S}_{3.875}$ appears to be an itinerant-electron ferrimagnet, which qualitatively explains the experimental observation of a slight FM polarization. Failure of a quantitative explanation could arise from the supercell approximation, because the actual sulfur vacancies are randomly distributed.

One also notes that, compared with the case of stoichiometric Co_3S_4 , E_F shifts to the right by $\sim 0.05 \text{ eV}$ [Fig. 6(d)]. This is consistent with the electron doping from the sulfur vacancy. The $N(E_F)$ value is increased to $4.2 \text{ eV}^{-1} \text{ f.u.}^{-1}$ based on both spins, corresponding to an electronic specific-heat coefficient of $\gamma_0 = 9.9 \text{ mJ K}^{-2} \text{ mol}^{-1}$. Nevertheless, it is still significantly lower than the experimental value, suggesting significant electron correlations in $\text{Co}_3\text{S}_{4-\delta}$. Theoretically, further increasing the electron correlations (via increasing U) would lead to a Mott-type metal-to-insulator transition, according to the phase diagram shown in Fig. 5.

IV. CONCLUDING REMARKS

We have studied the cobalt thiospinel $\text{Co}_3\text{S}_{4-\delta}$ experimentally and theoretically. Single-phase samples of $\text{Co}_3\text{S}_{4-\delta}$

were successfully prepared with sulfur deficiency of $\delta \sim 0.1$, avoiding formation of the undesired ferromagnetic impurity CoS_2 . The XRD Rietveld analysis confirms the sulfur deficiency. The magnetic, specific-heat, and electrical transport measurements demonstrate an AFM transition at $T_N \sim 60 \text{ K}$, above which SRO of Co(A) spins appears. The Curie-Weiss fitting for the high-temperature susceptibility data yields a small effective magnetic moment of $1.0 \mu_B$, indicative of an itinerant-electron scenario for the magnetism. The results of $\text{Co}_3\text{S}_{4-\delta}$ are set off by the NM analog $\text{NiCo}_2\text{S}_{3.9}$.

Our DFT calculations provide complementary information about the magnetic and electronic properties of $\text{Co}_3\text{S}_{4-\delta}$. We found that a small Hubbard U correction of $\sim 0.5 \text{ eV}$ is necessary to catch the experimental result. The calculations show that the Co(A)- t_2 orbitals are mostly occupied due to the t_2 - p hybridizations, which explains the reduced magnetic moment for the Co(A) ions. The AFM ordering slightly modifies the electronic structure. The sulfur deficiency of $\delta \sim 0.1$ generates uncompensated magnetic moments between the two interpenetrating lattices of the Co(A) site, and it shifts the Fermi level because of electron doping. Nevertheless, there are no remarkable changes on the ground-state properties. Compared with the bare electronic DOS from the DFT calculations, the experimental specific-heat coefficient is remarkably enhanced, indicating moderately strong electron correlations.

From the experimental measurements and theoretical calculations, We conclude that Co_3S_4 is an itinerant-electron weak antiferromagnet, rarely seen in a diamond lattice. Since this diamond-lattice antiferromagnetism is in the proximity of NM and FM states in energy, $\text{Co}_3\text{S}_{4-\delta}$ should be close to a magnetic QCP. As is known, peculiar phenomena such as non-Fermi-liquid behavior and unconventional superconductivity often emerge nearby a QCP [34–36]. Therefore, the present system might host exotic states of matter, which deserves further explorations with the

electronic states tuned by various chemical and physical methods.

ACKNOWLEDGMENTS

This work was supported by the National Natural Science Foundation of China (Grant No. 12050003) and the Key Research and Development Program of Zhejiang Province, China (Grant No. 2021C01002).

- [1] R. Stapele, Sulphospinels, *Handbook of Magnetic Materials* (North-Holland Publishing, Amsterdam, 1982), Vol. 3, pp. 603–745.
- [2] Q. Zhao, Z. Yan, C. Chen, and J. Chen, Spinels: Controlled preparation, oxygen reduction/evolution reaction application, and beyond, *Chem. Rev.* **117**, 10121 (2017).
- [3] V. Tsurkan, H.-A. Krug von Nidda, J. Deisenhofer, P. Lunkenheimer, and A. Loidl, On the complexity of spinels: Magnetic, electronic, and polar ground states, *Phys. Rep.* **926**, 1 (2021).
- [4] O. Knop, K. Reid, Sutarno, and Y. Nakagawa, Chalkogenides of the transition elements. VI. X-Ray, neutron, and magnetic investigation of the spinels Co_3O_4 , NiCo_2O_4 , Co_3S_4 , and NiCo_2S_4 , *Can. J. Chem.* **46**, 3463 (1968).
- [5] W. Roth, The magnetic structure of Co_3O_4 , *J. Phys. Chem. Solids* **25**, 1 (1964).
- [6] N. Tristan, V. Zestrea, G. Behr, R. Klingeler, B. Büchner, H. A. Krug von Nidda, A. Loidl, and V. Tsurkan, Spin frustration and magnetic exchange in cobalt aluminum oxide spinels, *Phys. Rev. B* **77**, 094412 (2008).
- [7] V. Fritsch, J. Hemberger, N. Büttgen, E.-W. Scheidt, H.-A. Krug von Nidda, A. Loidl, and V. Tsurkan, Spin and Orbital Frustration in MnSc_2S_4 and FeSc_2S_4 , *Phys. Rev. Lett.* **92**, 116401 (2004).
- [8] D. Bergman, J. Alicea, E. Gull, S. Trebst, and L. Balents, Order-by-disorder and spiral spin-liquid in frustrated diamond-lattice antiferromagnets, *Nature Phys.* **3**, 487 (2007).
- [9] F. L. Buessen, M. Hering, J. Reuther, and S. Trebst, Quantum Spin Liquids in Frustrated Spin-1 Diamond Antiferromagnets, *Phys. Rev. Lett.* **120**, 057201 (2018).
- [10] Y. Liu, C. Xiao, M. Lyu, Y. Lin, W. Cai, P. Huang, W. Tong, Y. Zou, and Y. Xie, Ultrathin Co_3S_4 nanosheets that synergistically engineer spin states and exposed polyhedra that promote water oxidation under neutral conditions, *Angew. Chem., Int. Ed.* **54**, 11231 (2015).
- [11] P. Ge, C. Zhang, H. Hou, B. Wu, L. Zhou, S. Li, T. Wu, J. Hu, L. Mai, and X. Ji, Anions induced evolution of Co_3X_4 ($X = \text{O}, \text{S}, \text{Se}$) as sodium-ion anodes: The influences of electronic structure, morphology, electrochemical property, *Nano Energy* **48**, 617 (2018).
- [12] R. Z. Wang and Y. Zhang, Magnetism modulation of Co_3S_4 towards the efficient hydrogen evolution reaction, *Mol. Syst. Des. Eng.* **5**, 565 (2020).
- [13] R. Samal, S. Mondal, A. S. Gangan, B. Chakraborty, and C. S. Rout, Comparative electrochemical energy storage performance of cobalt sulfide and cobalt oxide nanosheets: experimental and theoretical insights from density functional theory simulations, *Phys. Chem. Chem. Phys.* **22**, 7903 (2020).
- [14] R. F. Heidelberg, A. H. Luxem, S. Talhouk, and J. J. Baniewicz, The magnetic susceptibilities of the cobalt-sulfur system, *Inorg. Chem.* **5**, 194 (1966).
- [15] M. G. Townsend, L. Ripley, and J. Horwood, Absence of magnetic order in cobalt monosulphide, *Physica Status Solidi (a)* **32**, K29 (1975).
- [16] R. Bouchard, P. Russo, and A. Wold, Preparation and electrical properties of some thiospinels, *Inorg. Chem.* **4**, 685 (1965).
- [17] H. Nishihara, T. Kanomata, T. Kaneko, and H. Yasuoka, Pulsed nuclear magnetic resonance of ^{59}Co in Co_3S_4 , *J. Appl. Phys.* **69**, 4618 (1991).
- [18] S. Miyazaki, M. Shirai, and N. Suzuki, Electronic band structure of antiferromagnetic spinel Co_3S_4 , *J. Magn. Magn. Mater.* **177–181**, 1367 (1998).
- [19] Y.-Y. Jin, S.-H. Sun, Y.-W. Cui, Q.-Q. Zhu, L.-W. Ji, Z. Ren, and G.-H. Cao, Bulk superconductivity and Pauli paramagnetism in nearly stoichiometric CuCo_2S_4 , *Phys. Rev. Mater.* **5**, 074804 (2021).
- [20] C. Xia, P. Li, A. N. Gandi, U. Schwingenschlögl, and H. N. Alshareef, Is NiCo_2S_4 really a semiconductor? *Chem. Mater.* **27**, 6482 (2015).
- [21] F. Izumi and K. Momma, *Solid State Phenomena* (Trans Tech, Zurich, 2007), Vol. 130, pp. 15–20, doi: 10.4028/www.scientific.net/SSP.130.15.
- [22] P. E. Blöchl, Projector augmented-wave method, *Phys. Rev. B* **50**, 17953 (1994).
- [23] G. Kresse and J. Furthmüller, Efficient iterative schemes for ab initio total-energy calculations using a plane-wave basis set, *Phys. Rev. B* **54**, 11169 (1996).
- [24] J. P. Perdew, K. Burke, and M. Ernzerhof, Generalized Gradient Approximation Made Simple, *Phys. Rev. Lett.* **77**, 3865 (1996).
- [25] N. J. Mosey and E. A. Carter, Ab initio evaluation of Coulomb and exchange parameters for DFT + U calculations, *Phys. Rev. B* **76**, 155123 (2007).
- [26] N. Marzari and D. Vanderbilt, Maximally localized generalized Wannier functions for composite energy bands, *Phys. Rev. B* **56**, 12847 (1997).
- [27] K. Adachi, K. Sato, and M. Takeda, Magnetic properties of cobalt and nickel dichalcogenide compounds with pyrite structure, *J. Phys. Soc. Jpn.* **26**, 631 (1969).
- [28] The Curie-Weiss-like tails at low temperatures for the $\text{Co}_3\text{S}_{3.88}$ and $\text{NiCo}_2\text{S}_{3.9}$ samples are, respectively, equivalent to 3% and 6% paramagnetic impurities/defects with a localized spin of $S = 1/2$ (or, an effective moment of $1.73 \mu_B$). Since there are

- no Curie-Weiss-type paramagnetic phases at low temperatures reported in the Co-S and Ni-Co-S systems, we speculate that the susceptibility tails could be from those localized moments due to the sulfur vacancies.
- [29] G. A. Bain and J. F. Berry, Diamagnetic corrections and Pascal's constants, *J. Chem. Edu.* **85**, 532 (2008).
- [30] F. K. Lotgering and R. P. van Stapele, Magnetic properties and electrical conduction of copper-containing sulfo- and selenospinel, *J. Appl. Phys.* **39**, 417 (1968).
- [31] V. Anand and D. C. Johnston, Physical properties of EuPd_2As_2 single crystals, *J. Phys.: Condens. Matter* **26**, 286002 (2014).
- [32] I. Kim, H.-H. Nahm, and M. Choi, First-principles study of antiferromagnetic cobalt spinels, *Curr. Appl. Phys.* **22**, 65 (2021).
- [33] S. K. Kwon, S. J. Youn, and B. I. Min, Itinerant ferromagnetism in half-metallic CoS_2 , *Phys. Rev. B* **62**, 357 (2000).
- [34] P. Coleman and A. J. Schofield, Quantum criticality, *Nature (London)* **433**, 226 (2005).
- [35] S. Jiang, H. Xing, G. Xuan, C. Wang, Z. Ren, C. Feng, J. Dai, Z. Xu, and G. Cao, Superconductivity up to 30 K in the vicinity of the quantum critical point in $\text{BaFe}_2(\text{As}_{1-x}\text{P}_x)_2$, *J. Phys.: Condens. Matter* **21**, 382203 (2009).
- [36] B. Shen, Y. Zhang, Y. Komijani, M. Nicklas, R. Borth, A. Wang, Y. Chen, Z. Nie, R. Li, X. Lu, H. Lee, M. Smidman, F. Steglich, P. Coleman, and H. Yuan, Strange-metal behaviour in a pure ferromagnetic Kondo lattice, *Nature (London)* **579**, 51 (2020).